A Novel Conversion Vector-Based Low-Complexity SLM Scheme for PAPR Reduction in FBMC/OQAM Systems

Xing Cheng, *Member, IEEE*, Dejun Liu, *Member, IEEE*, Wenzhe Shi, Yang Zhao, Yang Li, and Dejin Kong

***Abstract*—Filter bank multicarrier with offset quadrature amplitude modulation (FBMC/OQAM) is considered as a powerful supplementary waveform for future wireless communications. However, FBMC systems have the same high peak-to-average power ratio (PAPR) problem as other multi-carrier systems, and the PAPR reduction methods designed for orthogonal frequency division multiplexing (OFDM) systems cannot be directly applied to FBMC systems due to the unique overlapping structure of FBMC signals. Therefore, some PAPR suppression schemes tailored to FBMC systems have been proposed, but their computational complexity is prohibitively high for some practical applications. In this paper, we propose a conversion vector-based low-complexity dispersive selection mapping (DSLM) scheme, called the C-DSLM scheme, to reduce the PAPR of FBMC signals. In the C-DSLM scheme, a series of conversion vectors is first carefully designed for FBMC signals with overlapping structures, and then candidate signals are generated by multiplying the original signal by the cyclic shift of the conversion vectors with only a few nonzero elements. The complexity evaluation and simulation results show that the C-DSLM scheme's PAPR suppression performance is similar to that of the DSLM scheme with computational complexity is only approximately 10% of that of the DSLM scheme. Our proposed C-DSLM scheme is highly efficient and strongly applicable.**

***Index Terms*—Filter bank multicarrier (FBMC), offset quadrature amplitude modulation (OQAM), selective mapping method (SLM), peak-to-average power ratio (PAPR), low complexity.**

Manuscript received July 24, 2019; revised November 13, 2019; accepted January 21, 2020. Date of publication March 16, 2020; date of current version September 3, 2020. This work was supported in part by the Research and Development of Key Instruments and Technologies for Deep Resources Prospecting (the National Research and Development Projects for Key Scientific Instruments) under Grant ZDYZ2012-1-07-02-01, and in part by the National Natural Science Foundation of China under Grant 41374151 and Grant 41074099. *(Corresponding author: Dejun Liu.)*

Xing Cheng is with the College of Information Science and Engineering, China University of Petroleum, Beijing 102249, China, and also with the School of Information and Communication Engineering, Beijing Information Science and Technology University, Beijing 100101, China (e-mail: 1123540775@qq.com).

Dejun Liu, Wenzhe Shi, Yang Zhao, and Yang Li are with the College of Information Science and Engineering, China University of Petroleum, Beijing 102249, China (e-mail: liudj65@163.com; 2637524104@qq.com; 982836762@qq.com; 1137712887@qq.com).

Dejin Kong is with the School of Electronic and Electrical Engineering, Wuhan Textile University, Wuhan 430074, China (e-mail: djkou@wtu.edu.cn).

Color versions of one or more of the figures in this article are available online at http://ieeexplore.ieee.org.

Digital Object Identifier 10.1109/TBC.2020.2977548

I. Introduction

In the future, wireless communication systems will serve a variety of application scenarios simultaneously in a common framework. For example, fifth-generation (5G) mobile communication will support three major types of application: enhanced mobile broadband (eMBB), massive machine-type communication (mMTC), and ultra-reliable, low latency communication (uRLLC) [1]. Orthogonal frequency division multiplexing (OFDM), which has been adopted as the standard waveform for many contemporary wireless communication systems, will remain in use in 5G systems because of its high compatibility with existing communication systems and because of the high cost of deploying a new system. However, OFDM has some drawbacks, such as low spectral efficiency, a high sidelobe spectrum, and inflexible modulation parameters adjustment (these modulation parameters include the subcarrier spacing, bandwidth, etc.), which make it difficult to meet the needs of all application scenarios [1]–[3]. Especially in emerging applications such as the Internet of Things (IoT) and gigabit connectivity, transmission is usually asynchronous, the spectrum is discontinuous, the packets are small, and low latency is required [2], [3]. Filter bank multicarrier with offset quadrature amplitude modulation (FBMC/OQAM), abbreviated as FBMC, which employs a nonrectangular prototype filter with good time-frequency focusing characteristics, has many features, such as low spectral sidelobes, high spectrum efficiency, flexible modulation parameters adjustment and low sensitivity to time synchronization [2]–[7]. It is worth noting that FBMC itself has low sensitivity to time synchronization; while OFDM requires a cyclic prefix (CP) with appropriate length and the additional symbol timing estimation algorithm, such as the two algorithms proposed respectively in [8] and [9], to obtain the characteristic of low sensitivity to time synchronization. In contrast to OFDM, FBMC systems are well suited to the needs of these application scenarios; therefore, FBMC is considered a powerful complementary waveform for future wireless communications.

However, FBMC systems also have some shortcomings, such as the difficulty of channel estimation due to inherent imaginary interference [10]–[12] and the high peak-to-average power ratio (PAPR) [13]. This paper focuses on the high PAPR of FBMC signals. A high PAPR means that some of the FBMC signals are outside the linear range of the high-power

amplifier (HPA), which causes serious nonlinear in-band and out-of-band signal distortion. The out-of-band distortion of the signal destroys the low sidelobes of the FBMC system, and the in-band nonlinear distortion of the signal increases the bit error rate (BER) of the FBMC system to some extent. Therefore, in an FBMC system, it is particularly important to suppress high PAPR to avoid performance degradation. Since the OFDM system that has been thoroughly studied also has issues with high PAPR, it is reasonable to modify and extend the PAPR suppression methods used with the OFDM system to the FBMC system. For the OFDM system, there are many PAPR suppression schemes [14], [15]. These can be classified into signal distortion classes, such as clipping filtering [16] and compression transformation [17]; non-signal distortion classes, such as partial transmission sequence (PTS) [18], selective mapping (SLM) [19], and tone reservation (TR) [20]; and coding classes, such as block coding [21], cyclic coding [22] and fountain coding [23].

Unfortunately, due to the unique overlapping structure of FBMC signals, the PAPR reduction methods designed for OFDM systems cannot be directly applied to FBMC systems. Therefore, many PAPR suppression schemes [24]–[41] specifically designed for FBMC systems have been proposed in succession. In general, all of these schemes are modifications of the PAPR reduction schemes for OFDM systems. Therefore, they can be classified into the following three categories: *Signal distortion category:* In [24], a clipping and iterative compensation scheme was proposed in which a time-domain signal was clipped and then an iterative noise cancellation technique was applied at the receiver to compensate the clipped signal. In [25], a nonlinear compounding scheme that converted the original signal to a new signal with a trapezoidal power distribution and then, using a flexible parameter, reduced the high PAPR of the FBMC signal was proposed. However, these schemes cause out-of-band distortion of the system alongside the lower PAPR of the FBMC signal. However, the extremely low out-of-band radiation is one of the key reasons for FBMC to become a candidate waveform in the future wireless communications. *Probabilistic category:* The probabilistic PAPR reduction schemes mainly include modified PTS-based schemes [26]–[29] and modified SLM-based schemes [30]–[35]. Among them, the dispersive selection mapping (DSLM) scheme proposed in [32] accounts for PAPR suppression performance and computational complexity simultaneously; details of its principle are provided in Section III-C. Although these probabilistic schemes do not decrease the excellent time-frequency focusing performance of an FBMC system, they are too computationally complex. *Hybrid category:* In general, there is no conflict between these types of PAPR suppression scheme, which makes it possible to combine two of the above schemes into a new hybrid scheme to obtain better PAPR suppression [2]; examples include some of the hybrid schemes proposed in [36]–[41]. However, the hybrid schemes are usually very computationally complex and easily cause out-of-band distortion to the system, which in turn weakens the time-frequency focusing of the FBMC system.

In summary, these PAPR suppression schemes are very computationally complex and impractical for some practical applications. For example, on-board batteries must be as durable as possible in machine-type communication (MTC), which inevitably requires an algorithm with low energy consumption to suppress the high PAPR [42]. In this paper, we propose a conversion vector-based low-complexity DSLM scheme, called the C-DSLM scheme, to reduce the PAPR of an FBMC signal. We first design a set of conversion vectors with special structure for FBMC signals and then propose the C-DSLM scheme, in which the candidate signals are generated by multiplying the original signal by the cyclic shift of the conversion vectors. Note that there are no more than 4 nonzero elements in each conversion vector. Therefore, the process of generating an alternate signal requires only a few complex addition operations. The C-DSLM scheme is a truly practical PAPR reduction scheme for FBMC systems. Specifically, the C-DSLM scheme, which features low complexity, is suitable for communication scenarios such as MTC not only because of its low energy consumption but also because its low cost makes the equipment competitive in terms of price [42].

As an important complementary waveform for future wireless communications, FBMC has many key issues including PAPR reduction all need to be innovatively addressed. However, compared with OFDM, the PAPR reduction scheme for FBMC has not been sufficiently studied. The C-DSLM scheme proposed in this paper represents a useful contribution to addressing the important PAPR issue of FBMC systems. The main contributions of this paper are summarized below.

- We fully study the overlapping structure of FBMC signals and design a set of conversion vectors with only a few nonzero elements. As far as the authors know, this work is the first time the idea of generating alternative signals based on conversion vectors to reduce the high PAPR of FBMC signals has been proposed.
- We propose the C-DSLM scheme, in which candidate signals are generated by multiplying the original signal by the cyclic shift of the conversion vectors. The process of generating an alternate signal requires only a few complex addition operations, making the C-DSLM scheme an ideal low-complexity scheme to reduce the high PAPR of FBMC signals.
- We thoroughly simulate the proposed C-DSLM scheme, and the results show that the C-DSLM scheme performs similarly to the DSLM scheme in terms of PAPR reduction with much less computational complexity. To the best of our knowledge, the C-DSLM scheme is the first truly practical PAPR reduction scheme for FBMC systems that has strong application prospects.

The remainder of this paper is organized as follows: Section II provides a brief introduction of the model FBMC/OQAM system and the problem with the PAPR of an FBMC signal. Some related work is described in Section III, and our proposed C-DSLM scheme is described in Section IV. In Section V, the performances of our proposed C-DSLM scheme and the DSLM and SLM schemes are compared, and the simulation results are shown. Finally, conclusions are given in Section VI.

Notations: Vectors are denoted by bold lower-case letters, while matrices are denoted by bold capital letters. Superscripts

$(\cdot)^T$, $E[\,\cdot\,]$ and $\langle\cdot\rangle$ represent the transpose, expectation and inner product operators, respectively. The symbols $\odot$, $\otimes$ and $\mathbb{C}^{m\times n}$ denote the dot product, circular convolution and vector space of all $m\times n$ complex matrices, respectively. Furthermore, diag($\mathbf{x}$) represents a diagonal matrix with the sequence $\mathbf{x}$ along the main diagonal.

II. Problem Description

A. Expressing an FBMC/OQAM Signal With an Overlapping Structure

Unlike the complex-valued data carried by each subcarrier in OFDM, each subcarrier in an FBMC/OQAM system carries real-valued data. Specifically, the FBMC/OQAM signal is a superposition of M symbols, where M is an even number, and each symbol contains N subcarriers. First, the complex-valued sequence obtained by QAM modulation is serial-to-parallel converted into a data matrix $\mathbf{D} = [\mathbf{d}^0, \mathbf{d}^1, \ldots, \mathbf{d}^{\frac{M}{2}-1}] \in \mathbb{R}^{N\times\frac{M}{2}}$, where $\mathbf{d}^m$ is the mth data vector, $\mathbf{d}^m = [d_0^m, d_1^m, \ldots, d_{N-1}^m]^T$ [31]. d_n^m is the complex-valued data carried by the nth subcarrier of the mth QAM symbol, $d_n^m = a_n^m + jb_n^m$, where a_n^m and b_n^m are the real and imaginary parts of d_n^m, respectively. We redefine the data matrix $\tilde{\mathbf{D}} \in \mathbb{R}^{N\times M}$ with elements d_n^m assigned by the following equation:

$$d_n^m = \begin{cases} a_n^{m/2}, & m = 0, 2, 4, \ldots, M-2 \\ b_n^{(m-1)/2}, & m = 1, 3, 5, \ldots, M-1. \end{cases} \tag{1}$$

Then, the continuous-time FBMC/OQAM signal $s(t)$ is expressed as

$$s(t) = \sum_{m=0}^{M-1}\sum_{n=0}^{N-1} d_n^m \underbrace{e^{j\frac{\pi}{2}(m+n)} e^{j2\pi nt/T} g\left(t - m\frac{T}{2}\right)}_{g_{m,n}(t)} \tag{2}$$

where the basis pulse $g_{m,n}(t)$ is essentially a time-frequency (TF) offset version of the symmetric real-valued prototype filter $g(t)$ and the length of $g(t)$ is usually $L_g = LN$, where L denotes the overlap factor (its value is usually set to an even number greater than 4). The length of the prototype filter L_g is much greater than N, which causes the FBMC symbols to overlap, as shown in Fig. 1. The length of an FBMC signal comprising M superimposed symbols is $LT + (M-1)\frac{T}{2} = (L + \frac{M}{2} - \frac{1}{2})T$, where T is the period of one FBMC symbol. The prototype filter has an essential effect on the performance of the FBMC system, and the most popular prototype filter PHYDYAS was designed by Bellanger in [43]. In this paper, we employ the PHYDYAS filter as the prototype filter for the FBMC system.

To intuitively reveal the overlapping structure of the FBMC/OQAM symbols, we depict the power profiles of both OFDM and FBMC symbols in Fig. 2 [32], [33]. Based on the power profiles, three items can be observed. First, the power of an OFDM symbol is distributed within the current symbol period T, but the main power of an FBMC symbol affected by the prototype filter is distributed across the periods of two neighboring symbols, i.e., $[T, 3T]$. Second, each FBMC symbol primarily overlaps with its two preceding and two subsequent symbols, especially its immediately previous and following symbols. Third, the peak value of the current FBMC symbol is influenced not only by the previous symbols but also by the subsequent symbols. These three observations play an important role in the design of the PAPR suppression scheme for FBMC systems, which is detailed later.

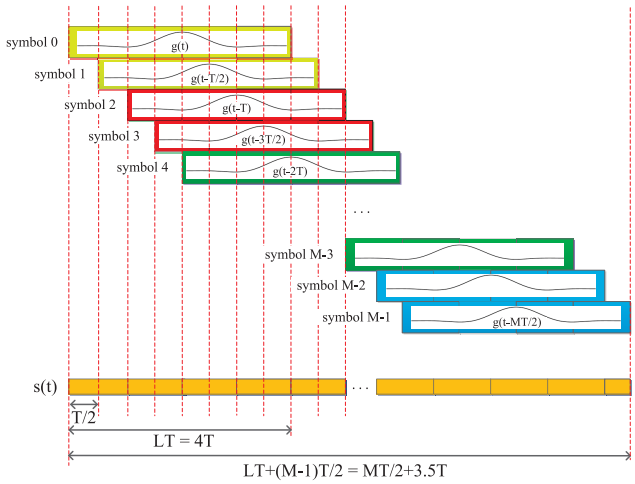

Fig. 1. Schematic of an FBMC/OQAM signal with an overlapping structure with $L = 4$.

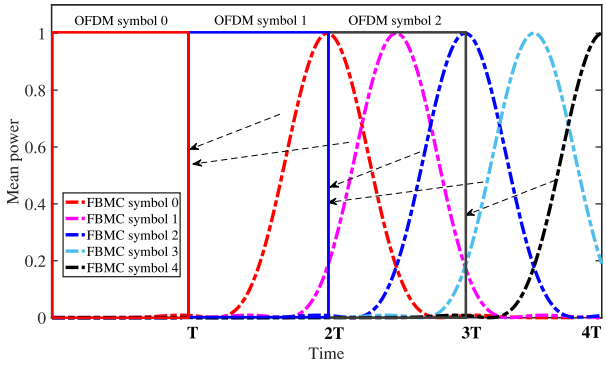

Fig. 2. Power profiles of OFDM and FBMC/OQAM symbols [32], [33].

B. The Definition of the PAPR in an FBMC/OQAM System

The symbols in an FBMC/OQAM signal overlap, and the length of an FBMC signal $LT + (M-1)\frac{T}{2}$ is much greater than T; therefore, the PAPR is defined differently for FBMC than for OFDM. An FBMC signal $s(t)$ to be transmitted must be divided into several intervals with a period of T. Then, the PAPR is calculated for each interval using the following formula [38]:

$$PAPR(s(t)) = 10\lg\frac{\max_{iT\le t\le(i+1)T}|s(t)|^2}{E\left[|s(t)|^2\right]}(\text{dB}). \tag{3}$$

To accurately reflect the fluctuation and peak distribution of the transmitted signal, the signal must be oversampled. Research has shown that an oversampling factor $O \ge 4$ suffices obtain an accurate PAPR for a discrete time signal [20]. According to basic knowledge of digital signal processing, the process of O-time oversampling in the time domain can be simulated by inserting $(O-1)\cdot N$ zero values in the middle

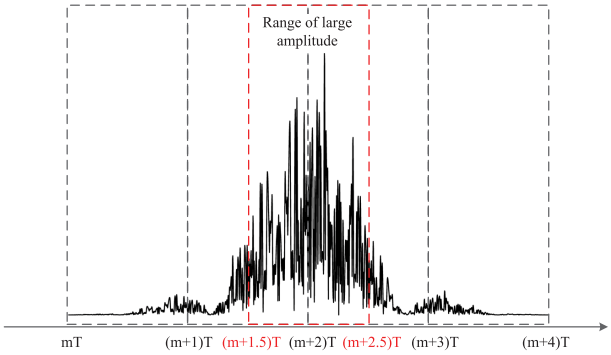

Fig. 3. Amplitude diagram of a time-domain FBMC/OQAM symbol with overlap factor $L = 4$.

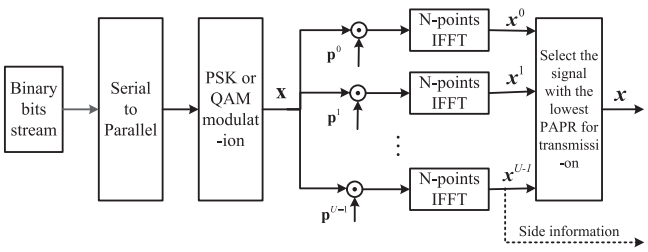

Fig. 4. Block diagram of the SLM scheme.

or at the end of the sequence in the frequency domain. The complementary cumulative distribution function (CCDF) is an important and common indicator used to evaluate the PAPR of a signal. It reflects the probability that the PAPR exceeds a threshold Z, i.e., $Pr\{PAPR(s(t)) > Z\}$. Fig. 3 shows an amplitude diagram of a time-domain FBMC/OQAM symbol.

III. Related Work

A. SLM Scheme

Fig. 4 shows a block diagram of the SLM scheme [19]. The data block $\mathbf{x} = [X[0], X[1], \ldots, X[N-1]]$ is multiplied by U corresponding phase rotation sequences $\mathbf{p}^u = [p_0^u, p_1^u, \ldots, p_{N-1}^u]$ $(u = 1, 2, \ldots, U)$, where $p_v^u = e^{j\theta_v^u}$ $(v = 0, 1, \ldots, N-1)$, $\theta_v^u \in [0, 2\pi)$. U modified sequences $\mathbf{x}^u = \mathbf{p}^u \odot \mathbf{x} = [p_0^u \cdot X[0], p_1^u \cdot X[1], \ldots, p_{N-1}^u \cdot X[N-1]]$ are obtained. The time-domain symbol $\boldsymbol{x}^u = [x^u[0], x^u[1], \ldots, x^u[N-1]]$ is obtained by applying the inverse fast Fourier transform (IFFT) to the u-th independent frequency-domain sequence $\mathbf{x}^u$. The OFDM signal $\boldsymbol{x}^{\tilde{u}}$ with the lowest PAPR is selected for transmission; note that some more efficient metrics, such as the distortion-to-signal power ratio (DSR) and cross correlation proposed respectively in [44] and [45], can also be used to select the optimal phase rotation sequence in the SLM scheme. The index $\tilde{u}$ is calculated according to the following equation (4):

$$\tilde{u} = \arg \min_{u=1,2,\ldots,U} \big(PAPR\big(\boldsymbol{x}^u\big)\big). \tag{4}$$

To correctly recover the original signal at the receiver, the index $\tilde{u}$ of the selected phase rotation sequence $\mathbf{p}^u$ should be sent to the receiver as side information (SI), which decreases the data throughput. In addition, U IFFT operations are needed in the SLM scheme. In general, the necessity of transmitting SI and high computational complexity are two shortcomings of the SLM scheme.

To decrease the complexity of the SLM scheme, θ_v^u is limited to $\{0, \pi\}$, i.e., $p_v^u \in \{1, -1\}$. Therefore, the selection of a phase rotation sequence in SLM can be abstracted into a combinatorial optimization problem:

$$(\mathrm{P1}) : \mathbf{p}^{\tilde{u}} = \arg \min_{u=1,\ldots,U} \big\{PAPR\big(\mathrm{IFFT}\big(\mathbf{p}^u \odot \mathbf{x}\big)\big)\big\}. \tag{5}$$

The optimal solution to this problem (P1) is to perform all combinations, i.e., $U = 2^N$ and then select the best one. However, the amount of computation increases exponentially with the number of subcarriers. For example, when the number of subcarriers $N = 512$, the total number of combinations is astronomical. Accordingly, the usual practice of the SLM scheme is to randomly generate U (4, 8 or 16) independent phase rotation sequences and then select the sequence that results in the lowest PAPR for the OFDM signal.

B. CSLM Scheme for OFDM Systems

Although the traditional SLM scheme described above adopts a suboptimal method to decrease its computational complexity, it requires U IFFT operations, which means its complexity remains too high. To further decrease the complexity of the traditional SLM scheme, the authors of [46] first proposed a conversion vector-based SLM (CSLM) scheme to reduce the PAPR of the OFDM signal.

In the CSLM scheme, some of the candidate signals are generated by cyclic shift multiplication of the time-domain OFDM signal and the conversion vectors, which allows some IFFT operations to be avoided. A schematic for generating candidate OFDM symbols based on the conversion vectors is shown in Fig. 5, which visualizes the following equations (6) and (7) [47]:

$$\boldsymbol{x} = \mathrm{IFFT}_N\{\mathbf{x}\} = \mathbf{F}\mathbf{x} \tag{6}$$

$$\boldsymbol{x}^u = \mathrm{IFFT}_N\big\{\mathbf{p}^u \odot \mathbf{x}^u\big\} = \mathbf{F}\mathbf{Q}^u\mathbf{x} \tag{7}$$

where $\mathbf{Q}^u$ denotes a diagonal matrix composed of elements in the phase rotation sequence $\mathbf{p}^u$, i.e., $\mathbf{Q}^u = diag(\mathbf{p}^u)$. $\mathbf{F}$ is the matrix form of the N-point IFFT transform.

$$\mathbf{F} = \frac{1}{N}\begin{pmatrix} 1 & 1 & 1 & \cdots & 1 \\ 1 & W_N^{-1} & W_N^{-2} & \cdots & W_N^{-(N-1)} \\ 1 & W_N^{-2} & W_N^{-4} & \cdots & W_N^{-2(N-2)} \\ \vdots & \vdots & \vdots & \ddots & \vdots \\ 1 & W_N^{-(N-1)} & W_N^{-2(N-1)} & \cdots & W_N^{-(N-1)(N-1)} \end{pmatrix} \tag{8}$$

where $W_N = e^{-j2\pi/N}$. The inverse of equation (6) can be written as

$$\mathbf{x} = \mathbf{F}^{-1}\boldsymbol{x} \tag{9}$$

where $\mathbf{F}^{-1}$ denotes the FFT. Therefore, equation (7) can be rewritten as

$$\boldsymbol{x}^u = \mathbf{F}\mathbf{Q}^u\mathbf{F}^{-1}\boldsymbol{x} = \mathbf{C}^u\boldsymbol{x} \tag{10}$$

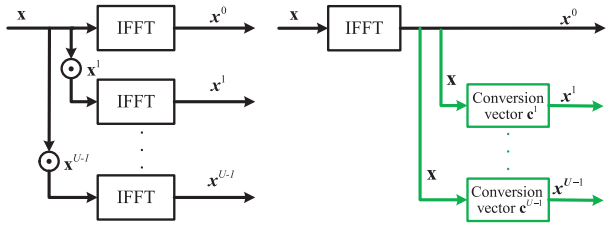

Fig. 5. Schematic for generating candidate OFDM symbols based on the conversion vectors.

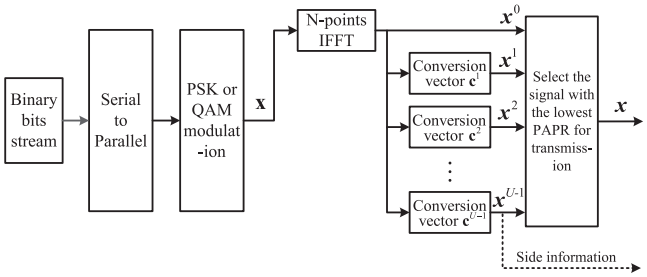

Fig. 6. Block diagram of the CSLM scheme.

where $\mathbf{C}^u = \mathbf{F}\mathbf{Q}^u\mathbf{F}^{-1}$ denotes the conversion matrix, which is explained later. Equation (10) shows that a candidate signal $\boldsymbol{x}^u$ can be generated directly from the time-domain signal $\boldsymbol{x}$. It now appears that constructing the conversion matrix $\mathbf{C}^u$ is the key issue in the CSLM scheme.

Using the properties of circular convolution in digital signal processing, the following equation can be obtained:

$$\boldsymbol{x}^u = \mathrm{IFFT}_N\left\{\mathbf{p}^u \odot \mathbf{x}^u\right\} = \left(\mathbf{F}\mathbf{p}^u\right) \otimes_N (\mathbf{F}\mathbf{x}) = \mathbf{c}^u \otimes_N \boldsymbol{x} \quad (11)$$

where $\otimes_N$ denotes N-point circular convolution. Comparing equations (10) and (11) leads to the conversion matrix $\mathbf{C}^u$ via the following formula:

$$\mathbf{C}^u = \left[\left(\mathbf{c}^u\right)^{\langle 0\rangle}, \left(\mathbf{c}^u\right)^{\langle 1\rangle}, \ldots, \left(\mathbf{c}^u\right)^{\langle N-1\rangle}\right] \quad (12)$$

where $(\mathbf{c}^u)^{\langle n\rangle}$, $n = 0, 1, 2, \ldots, N-1$ denotes a column vector obtained by cyclically shifting the time-domain sequence $\mathbf{c}^u$ downward n positions. $\mathbf{c}^u$ is also called a conversion vector and obtained by taking the IFFT of the phase rotation sequence $\mathbf{p}^u$, i.e., $\mathbf{c}^u = \mathbf{F}\mathbf{p}^u$, as shown in equation (11). The authors of [46]–[49] have ingeniously designed special phase rotation sequences $\mathbf{p}^u$, and the corresponding conversion vectors $\mathbf{c}^u$ have no more than four nonzero elements (the real and imaginary parts of these elements are from the set $\{\pm 1, 0\}$). An example is the phase rotation sequence $\mathbf{p}^u = 2 \times [\underline{1, j, 1, -j}, \underline{1, j, 1, -j}, \ldots, \underline{1, j, 1, -j}]^T$ given in [48] and the corresponding conversion vector $\mathbf{c}^u = [\underline{1, 0, \ldots, 0}, \underline{-1, 0, \ldots, 0}, \underline{1, 0, \ldots, 0}, \underline{1, 0, \ldots, 0}]^T$. As a result, the circular convolution of $\mathbf{c}^u$ and $\boldsymbol{x}$ requires no complex multiplication and only $3N$ complex addition operations. Therefore, the computational complexity of the CSLM scheme is much lower than that of the traditional SLM scheme. A block diagram of the CSLM scheme is shown in Fig. 6.

C. DSLM Scheme for FBMC Systems

To reduce the PAPR of an FBMC signal with an intrinsic overlapping structure, a dispersive SLM (DSLM) scheme was proposed in [32]. In the DSLM scheme, the manner of generating the rotated candidate symbols is similar to that of the traditional SLM scheme and requires U IFFTs, making it very complex. The traditional SLM scheme designed for OFDM signals only needs to consider the current symbol when selecting the optimal rotation sequence. In contrast, when selecting the optimal rotation sequence, the DSLM scheme should consider not only the current symbol but also the influence of several past symbols that overlap with it. For example, for the current mth symbol, the optimal phase rotation sequence is determined by the PAPR of the following signal on the interval T_0

$$s^u(t) = \underbrace{\sum_{m'=0}^{2m-1}\sum_{n=0}^{N-1} x_{m',n}^{u_{min}} g\left(t - m'\frac{T}{2}\right) e^{j\frac{2\pi}{T}nt} e^{j\phi_{m',n}}}_{\text{overlapping past symbols}} + \underbrace{\sum_{m'=2m}^{2m+1}\sum_{n=0}^{N-1} x_{m',n}^{u} g\left(t - m'\frac{T}{2}\right) e^{j\frac{2\pi}{T}nt} e^{j\phi_{m',n}}}_{\text{current symbol}}. \quad (13)$$

In equation (13), $0 \le m \le M-1$, $0 \le u \le U-1$, where $s^u(t) \neq 0$ when $t = [0, (2m+1)T + 4T]$ and $x_{m',n}^{u_{min}}$ are chosen from the previously selected symbols $C_m^{u_{min}}$. The PAPR of the signal $s^u(t)$ is calculated on the interval $T_0 = [mT, mT + 4T]$. Note that the choice of the interval T_0 plays a crucial role in the PAPR suppression performance of the DSLM scheme [32]. If $T_0 = [mT, mT + T]$, then the overlapping structure of the FBMC signal is not considered at all, and the DSLM scheme does not reduce the PAPR, which is easy to understand intuitively. The numerical simulation results in Section V confirm this intuition.

IV. Proposed Low-Complexity C-DSLM Scheme for FBMC/OQAM Systems

In this section, we propose a conversion vector-based low-complexity DSLM (C-DSLM) scheme to reduce the PAPR of an FBMC/OQAM signal. We first design and construct the conversion vectors, and then we describe the specific steps in the C-DSLM scheme. Finally, we evaluate its computational complexity.

A. The Design of the Conversion Vectors

Because phase rotation is applied to the frequency-domain data after OQAM modulation in this paper, the phase rotation factors must be real-valued to avoid destroying the interleaved structure of the real- and imaginary-valued data. In addition, to ensure that the computational complexity that does not exceed that of the CSLM scheme, which requires no multiplication and $3N$ complex addition operations, the elements in the conversion vector $\mathbf{c}^u$ obtained by taking the IFFT of the phase rotation vector $\mathbf{p}^u$ should come from the set $\{\pm 1, \pm j\}$. In summary, the expected conversion vector $\mathbf{c}^u$ should satisfy the following two conditions:

$$\mathbf{C}^3 = 0.5 \times \begin{pmatrix} 1 & 0 & 0 & 0 & j & 0 & 0 & 0 & 1 & 0 & 0 & 0 & -j & 0 & 0 & 0 \\ 0 & 1 & 0 & 0 & 0 & j & 0 & 0 & 0 & 1 & 0 & 0 & 0 & -j & 0 & 0 \\ 0 & 0 & 1 & 0 & 0 & 0 & j & 0 & 0 & 0 & 1 & 0 & 0 & 0 & -j & 0 \\ 0 & 0 & 0 & 1 & 0 & 0 & 0 & j & 0 & 0 & 0 & 1 & 0 & 0 & 0 & -j \\ -j & 0 & 0 & 0 & 1 & 0 & 0 & 0 & j & 0 & 0 & 0 & 1 & 0 & 0 & 0 \\ 0 & -j & 0 & 0 & 0 & 1 & 0 & 0 & 0 & j & 0 & 0 & 0 & 1 & 0 & 0 \\ 0 & 0 & -j & 0 & 0 & 0 & 1 & 0 & 0 & 0 & j & 0 & 0 & 0 & 1 & 0 \\ 0 & 0 & 0 & -j & 0 & 0 & 0 & 1 & 0 & 0 & 0 & j & 0 & 0 & 0 & 1 \\ 1 & 0 & 0 & 0 & -j & 0 & 0 & 0 & 1 & 0 & 0 & 0 & j & 0 & 0 & 0 \\ 0 & 1 & 0 & 0 & 0 & -j & 0 & 0 & 0 & 1 & 0 & 0 & 0 & j & 0 & 0 \\ 0 & 0 & 1 & 0 & 0 & 0 & -j & 0 & 0 & 0 & 1 & 0 & 0 & 0 & j & 0 \\ 0 & 0 & 0 & 1 & 0 & 0 & 0 & -j & 0 & 0 & 0 & 1 & 0 & 0 & 0 & j \\ j & 0 & 0 & 0 & 1 & 0 & 0 & 0 & -j & 0 & 0 & 0 & 1 & 0 & 0 & 0 \\ 0 & j & 0 & 0 & 0 & 1 & 0 & 0 & 0 & -j & 0 & 0 & 0 & 1 & 0 & 0 \\ 0 & 0 & j & 0 & 0 & 0 & 1 & 0 & 0 & 0 & -j & 0 & 0 & 0 & 1 & 0 \\ 0 & 0 & 0 & j & 0 & 0 & 0 & 1 & 0 & 0 & 0 & -j & 0 & 0 & 0 & 1 \end{pmatrix} \tag{14}$$

Fig. 7. The example conversion matrix $\mathbf{C}^3$ shows the downward cyclic shift structure.

TABLE I
ALL 16 TYPES OF PHASE ROTATION VECTOR TUPLE $\tilde{\mathbf{p}}^u$ AND THE CORRESPONDING CONVERSION VECTOR TUPLES $\tilde{\mathbf{c}}^u$

Index	Phase rotation vector tuple	Conversion vector tuple
1	$\tilde{\mathbf{p}}^1$ = [1 1 1 1]	$\tilde{\mathbf{c}}^1$ = [1 0 0 0]
2	$\tilde{\mathbf{p}}^2$ = [-1 1 1 1]	$\tilde{\mathbf{c}}^2$ = [1 -1 -1 -1]
3	$\tilde{\mathbf{p}}^3$ = [1 -1 1 1]	$\tilde{\mathbf{c}}^3$ = [1 -j 1 j]
4	$\tilde{\mathbf{p}}^4$ = [-1 -1 1 1]	$\tilde{\mathbf{c}}^4$ = [0 -1-j 0 -1+j]
5	$\tilde{\mathbf{p}}^5$ = [1 1 -1 1]	$\tilde{\mathbf{c}}^5$ = [1 1 -1 1]
6	$\tilde{\mathbf{p}}^6$ = [-1 1 -1 1]	$\tilde{\mathbf{c}}^6$ = [0 0 -1 0]
7	$\tilde{\mathbf{p}}^7$ = [1 -1 -1 1]	$\tilde{\mathbf{c}}^7$ = [0 1-j 0 1+j]
8	$\tilde{\mathbf{p}}^8$ = [-1 -1 -1 1]	$\tilde{\mathbf{c}}^8$ = [-1 -j -1 j]
9	$\tilde{\mathbf{p}}^9$ = -[-1 -1 -1 1] = $-\tilde{\mathbf{p}}^8$	$\tilde{\mathbf{c}}^9$ = -[-1 -j -1 j] = $-\tilde{\mathbf{c}}^8$
10	$\tilde{\mathbf{p}}^{10}$ = -[1 -1 -1 1] = $-\tilde{\mathbf{p}}^7$	$\tilde{\mathbf{c}}^{10}$ = -[0 1-j 0 1+j] = $-\tilde{\mathbf{c}}^7$
11	$\tilde{\mathbf{p}}^{11}$ = -[-1 1 -1 1] = $-\tilde{\mathbf{p}}^6$	$\tilde{\mathbf{c}}^{11}$ = -[0 0 -1 0] = $-\tilde{\mathbf{c}}^6$
12	$\tilde{\mathbf{p}}^{12}$ = -[1 1 -1 1] = $-\tilde{\mathbf{p}}^5$	$\tilde{\mathbf{c}}^{12}$ = -[1 1 -1 1] = $-\tilde{\mathbf{c}}^5$
13	$\tilde{\mathbf{p}}^{13}$ = -[-1 -1 1 1] = $-\tilde{\mathbf{p}}^4$	$\tilde{\mathbf{c}}^{13}$ = -[0 -1-j 0 -1+j] = $-\tilde{\mathbf{c}}^4$
14	$\tilde{\mathbf{p}}^{14}$ = -[1 -1 1 1] = $-\tilde{\mathbf{p}}^3$	$\tilde{\mathbf{c}}^{14}$ = -[1 -j 1 j] = $-\tilde{\mathbf{c}}^3$
15	$\tilde{\mathbf{p}}^{15}$ = -[-1 1 1 1] = $-\tilde{\mathbf{p}}^2$	$\tilde{\mathbf{c}}^{15}$ = -[1 -1 -1 -1] = $-\tilde{\mathbf{c}}^2$
16	$\tilde{\mathbf{p}}^{16}$ = -[1 1 1 1] = $-\tilde{\mathbf{p}}^1$	$\tilde{\mathbf{c}}^{16}$ = -[1 0 0 0] = $-\tilde{\mathbf{c}}^1$

1) The number of nonzero elements in the conversion vector $\mathbf{c}^u$ must not exceed 4.
2) The real and imaginary parts of the nonzero elements in the conversion vector $\mathbf{c}^u$ should be selected from the set $\{1, -1, 0\}$ (ignoring the constant factor of 1/2).

We obtain the inverse negative of the **Theorem** proposed and proven in [48], that is, let $\mathbf{p}^u$ be a phase rotation vector of length N (N is a power of 2) with all elements belonging to the set $\{1, -1\}$. If the real and imaginary parts of all elements of $\mathbf{c}^u = \text{IFFT}\{\mathbf{p}^u\}$ are in the set $\{1, -1, 0\}$, the minimum period D of a sequence $\mathbf{p}^u$ of length N must be ≤ 8. This inverse negative proposition can guide us in constructing some conversion vectors that satisfy the above two conditions.

Set the minimum period D to 4, and fully combine 4 elements (whose values are equal to 1 or -1) to obtain 2^4 types of phase rotation vector tuple $\tilde{\mathbf{p}}$, as shown in Table I. Correspondingly, the conversion vector tuple $\tilde{\mathbf{c}}^u$ can be easily obtained by taking the IFFT of $\tilde{\mathbf{p}}^u$, i.e., $\tilde{\mathbf{c}}^u = \text{IFFT}\{\tilde{\mathbf{p}}^u\}$. By repeating the vector $\tilde{\mathbf{p}}^u$ $\frac{N}{D}$ times, we obtain the desired phase rotation vector $\mathbf{p}^u$, i.e., $\mathbf{p}^u = [(\tilde{\mathbf{p}}^u)^T, (\tilde{\mathbf{p}}^u)^T, \ldots, (\tilde{\mathbf{p}}^u)^T]^T$ [48]. Using $\tilde{\mathbf{p}}^3 = \{1, -1, 1, 1\}$ as an example yields

$$\mathbf{p}^3 = \left[\underline{1, -1, 1, 1}, \underline{1, -1, 1, 1}, \underbrace{\ldots}_{(\frac{N}{4}-3) \text{ times } \tilde{\mathbf{p}}^3}, \underline{1 - 1, 1, 1} \right] \tag{15}$$

$$\mathbf{c}^3 = \left[1, \underbrace{0, 0, \ldots, 0}_{\frac{N-4}{4}}, -j, \underbrace{0, 0, \ldots, 0}_{\frac{N-4}{4}}, 1, \underbrace{0, 0, \ldots, 0}_{\frac{N-4}{4}}, j, \underbrace{0, 0, \ldots, 0}_{\frac{N-4}{4}} \right]. \tag{16}$$

According to basic digital signal processing, multiplication in the frequency domain corresponds to convolution in the time domain. Therefore, the candidate time-domain signal $\mathbf{s}^u$ to be transmitted can be obtained by circular convolution of the time-domain sequence $\mathbf{s}$ and the conversion vector $\mathbf{c}^u$ [47]. This process can be expressed as the product of $\mathbf{s}$ and a cyclic convolution matrix $\mathbf{C}^u$, i.e., $\mathbf{s}^u = \mathbf{C}^u\mathbf{s}$, where $\mathbf{C}^u$, the convolution matrix corresponding to $\mathbf{c}^u$, can be expressed as

$$\mathbf{C}^u = \left[(\mathbf{c}^u)^{\langle 0 \rangle}, (\mathbf{c}^u)^{\langle 1 \rangle}, \ldots, (\mathbf{c}^u)^{\langle N-2 \rangle}, (\mathbf{c}^u)^{\langle N-1 \rangle} \right] \tag{17}$$

where $(\mathbf{c}^u)^{\langle n \rangle}$ represents the downward cyclic shift of $\mathbf{c}^u$ by n elements, and equation (14) shows this downward cyclic shift structure with $\mathbf{C}^3$ as an example.

B. Conversion Vector-Based DSLM Scheme (C-DSLM)

In the previous subsection, the necessary conversion vectors for the C-DSLM scheme are constructed. In this subsection, we describe the implementation of the C-DSLM scheme in detail.

1) *Initialization Phase:* Set the number of subcarriers N, the number of symbols M, the number of conversion vectors U, the overlap factor L, and the oversampling factor O. Initialize the symbol index to $m = 1$. Generate

the conversion matrix $\mathbf{C}^u$ using equations (18)-(20)

$$\mathbf{p}^u = \left[\underbrace{\left(\tilde{\mathbf{p}}^u\right)^T, \left(\tilde{\mathbf{p}}^u\right)^T, \ldots, \left(\tilde{\mathbf{p}}^u\right)^T}_{\text{Repeat } \frac{ON}{4} \text{ times}}\right]^T \in \mathbb{C}^{1\times \text{ON}} \tag{18}$$

$$\mathbf{c}^u = \text{IFFT}\{\mathbf{p}^u\} \in \mathbb{C}^{1\times \text{ON}} \tag{19}$$

$$\mathbf{C}^u = \left[\left(\mathbf{c}^u\right)^{\langle 0\rangle}, \left(\mathbf{c}^u\right)^{\langle 1\rangle}, \ldots, \left(\mathbf{c}^u\right)^{\langle ON-1\rangle}\right] \in \mathbb{C}^{\text{ON}\times \text{ON}} \tag{20}$$

where $u \in \{1, 2, \ldots, U\}$ is the phase rotation vector tuple $\tilde{\mathbf{p}}^u$ in (18), as shown in Table I.

2) *Conversion Vector-Based Modulation:* Inserting $(O-1)N$ zeros in the middle of the current frequency-domain vector $\mathbf{x}$, i.e., $\mathbf{x} = [x_1, x_2, \ldots, x_{\frac{N}{2}}, 0, 0, \ldots, 0, 0, x_{\frac{N}{2}+1}, x_{\frac{N}{2}+2}, \ldots, x_N]$, and taking the IFFT yields a candidate time-domain vector $\mathbf{s}^1$ oversampled O times. The remaining $U-1$ candidate vectors $\mathbf{s}$ are obtained with the following equation:

$$\mathbf{s}^u = \mathbf{C}^u \cdot \mathbf{s}^1 \in \mathbb{R}^{1\times \text{ON}}, u = 2, 3, \ldots, U. \tag{21}$$

Repeating $\mathbf{s}^u$ L times and multiplying it by the prototype filter g yields the FBMC/OQAM symbol,

$$\mathbf{s}_L^u = \left[\underbrace{\left(\mathbf{s}^u\right)^T, \left(\mathbf{s}^u\right)^T, \ldots, \left(\mathbf{s}^u\right)^T}_{\text{repeat L times}}\right]^T \in \mathbb{R}^{1\times \text{L}\cdot\text{ON}} \tag{22}$$

$$\mathbf{s}_m^u = \mathbf{s}_L \cdot g \in \mathbb{R}^{1\times \text{L}\cdot\text{ON}} \tag{23}$$

$$\mathbf{s}^u(t) = \underbrace{\sum_{m'=1}^{m-1} \mathbf{s}_{m'}^{u_{min}^{m'}}}_{\text{overlapping past symbols}} + \underbrace{\mathbf{s}_m^u}_{\text{current symbol}} \tag{24}$$

where $m' \in \{1, 2, \ldots, M-1\}$, $\mathbf{s}_{m'}^{u_{min}^{m'}}$ is the signal with the minimum PAPR of the U candidate signals from the previous round.

3) *PAPR Calculation:* Then, we compute the PAPR of $s^u(t)$ on a certain interval T_o,

$$PAPR_{T_0}^u = \frac{\max_{t\in T_0}|\mathbf{s}^u(t)|^2}{\frac{1}{T_0}\int_{T_0}|\mathbf{s}^u(t)|^2 dt}, u \in \{1, 2, \ldots, U\} \tag{25}$$

where the range of T_o seriously affects the PAPR reduction performance of the C-DSLM scheme. $T_0 = [mT, mT + 4T]$ since almost all of the symbol's energy is within an interval of size $4T$, as discussed in Section II-B.

4) *Selection:* Select the smallest of the U PAPRs obtained above and record its index number as u_{min}. This process is described by the following formula:

$$u_{min} = \min_{0\le u\le U-1} PAPR_{T_0}^u. \tag{26}$$

5) *Update:* Update the current overlapping input symbol vector,

$$\mathbf{s}_{m'+1}^{u_{min}^{m'+1}} = \mathbf{s}^{u_{min}}(t). \tag{27}$$

TABLE II
COMPUTATIONAL COMPLEXITY OF THE DSLM SCHEME AND OUR PROPOSED C-DSLM SCHEME

	Number of Multiplications	Number of Additions
DSLM scheme	$UM\frac{ON}{2}\log_2(ON)$	$UMON\log_2(ON)$
C-DSLM scheme	$M\frac{ON}{2}\log_2(ON)$	$MON\log_2(ON) + 3(U-1)MON$

The index u_{min} is stored in a vector **SI** to be transmitted as side information (SI) for perfectly recovering the transmitted data at the receiver;

$$\mathbf{SI} = [\mathbf{SI} \quad u_{min}]. \tag{28}$$

Then, $m = m + 1$, and **Step 2** is repeated to complete the operations for the next input symbol until $m = M$.

C. Complexity Evaluation

In this subsection, we evaluate the computational complexity of the C-DSLM scheme, which is measured by the number of multiplication and addition operations required. To quantify the reduction in computational complexity compared with that of the other schemes, we use the computational complexity reduction ratio (CCRR) metric introduced in [50], which is defined as

$$\text{CCRR} = \left(1 - \frac{\text{complexity of the C-DSLM scheme}}{\text{complexity of the DSLM scheme}}\right) \times 100\%. \tag{29}$$

Analyzing all the steps of the C-DSLM scheme described in the previous subsection shows that the complexity mainly comes from the FFT and multiplication by the conversion matrix. An N-point IFFT requires $\frac{N}{2}\log_2 N$ complex multiplications and $N\log_2 N$ complex addition operations. In the C-DSLM scheme, only one IFFT is required for each symbol block, and the remaining $U-1$ IFFT operations are replaced by matrix multiplications. Since O-time oversampling is implemented using zero-padding in the frequency domain, the number of points in the IFFT is ON, so the M IFFTs in the C-DSLM scheme (the number of symbol blocks is M) only require $M\frac{ON}{2}\log_2(ON)$ complex multiplications and $MON\log_2(ON)$ complex addition operations. Shift multiplying by the conversion vector of length ON requires only $3ON$ complex addition operations because there are only 4 nonzero elements in each conversion vector, and all of these elements are in the set $\{1, -1\}$. In summary, our proposed C-DSLM scheme requires $M\frac{ON}{2}\log_2(ON)$ complex multiplication operations and $MON\log_2(ON)+3(U-1)MON$ complex addition operations, as shown in Table II. In contrast, in the DSLM scheme, each symbol block requires U IFFTs for a total of $UM\frac{ON}{2}\log_2(ON)$ complex multiplication operations and $UMON\log_2(ON)$ complex addition operations.

To quantitatively evaluate the complexity of the C-DSLM and DSLM schemes, we set the number of subcarriers N, the number of symbol blocks M, and the oversampling factor O to 64, 100, and 4, respectively. When the number of phase

TABLE III
NUMERICAL COMPARISON OF THE COMPUTATIONAL COMPLEXITY IN TABLE II FOR $M = 100$, $N = 64$, $U = 4, 8, 16$

	U = 4		U = 8		U = 16	
	Number of Multi-plications	Number of Addi-tions	Number of Multi-plications	Number of Addi-tions	Number of Multi-plications	Number of Addi-tions
DSLM scheme	409600	819200	819200	1638400	1638400	3276800
C-DSLM scheme	102400	435200	102400	742400	102400	1356800
CCRR	**75%**	46.9%	**87.5%**	54.7%	**93.8%**	58.6%

rotation vectors U is 4, 8, or 16, the numbers of complex multiplication and addition operations required for the C-DSLM and DSLM schemes are shown in Table III. The number of complex multiplications required for the C-DSLM scheme is decreased as much as 75% ($U = 4$), 87.5% ($U = 8$) and 93.8% ($U = 16$) of that of the DSLM scheme.

V. SIMULATION RESULTS

In this section, the proposed C-DSLM scheme is comprehensively and objectively simulated from the perspective of its ability to reduce the PAPR. The results are compared with those of existing PAPR reduction schemes designed for OFDM and FBMC/OQAM signals.

At the beginning of the simulation study, it is necessary to uniformly configure some parameters. The FBMC/OQAM signal is generated by 1.5×10^4 complex-valued 4-QAM modulated symbols, i.e., 3×10^4 OQAM real-valued symbols, the number of subcarriers N is set to 64, and the overlap factor L and the oversampling factor O are both set to 4. The PHYDYAS filter [43] is employed as the prototype filter, all the phase rotation factors p_v^u are selected from $\{1, -1\}$, and the sizes of the rotation vector U are set to 2, 4, and 8. To comprehensively evaluate the performance of the C-DSLM scheme in terms of PAPR reduction, we successively simulate the impacts of several factors, such as the size of U, PAPR calculation interval T_0, the number of subcarriers N and the type of prototype filter. Finally, we compare the C-DSLM scheme's performance in terms of PAPR reduction for FBMC signals with that of the conventional SLM scheme for OFDM signals.

A. Impact of the Size of U

First, we consider the impact of the value of U on the performance of the C-DSLM scheme. As mentioned in Section III-A, the greater U is, the better the SLM scheme is at reducing the PAPR, which is easy to understand intuitively. Our proposed C-DSLM scheme is based on the conventional SLM scheme, and both of them are probabilistic. The C-DSLM scheme certainly should satisfy this rule, and the simulation results confirm that it does. Fig. 8 shows the CCDF of the PAPR of an FBMC signal suppressed by the DSLM and C-DSLM schemes for different values of U. When CCDF

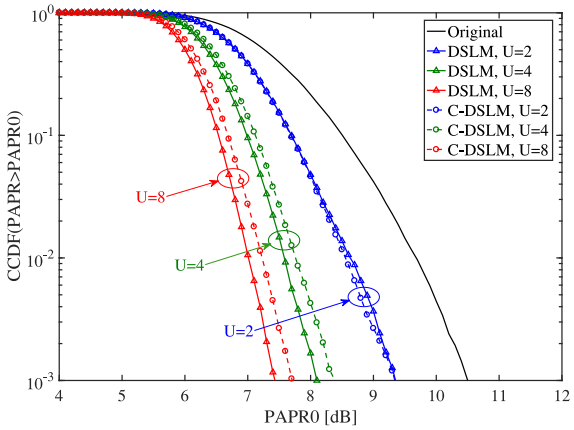

Fig. 8. CCDFs of the C-DSLM scheme for different values of U, i.e., $U = 2, 4, 8$; PHYDYAS filter, $N = 64$, $L = 4$, and $O = 4$.

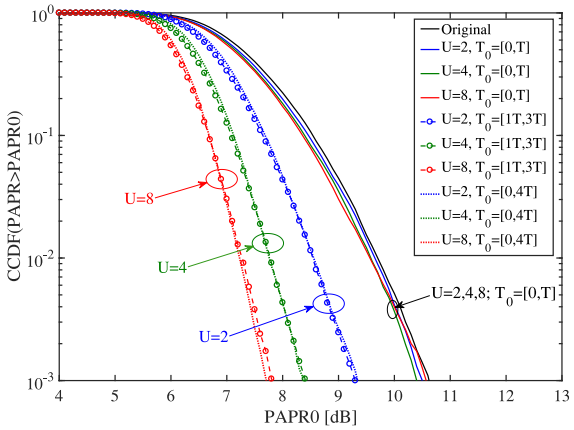

Fig. 9. CCDFs of the proposed C-DSLM scheme for different T_0, i.e., T_0 = [0, T], [1T, 3T], [0 4T]; $U = \{2, 4, 8\}$, $N = 64$, and $O = 4$.

$= 10^{-3}$ and U is equal to 2, the performance of the C-DSLM scheme is almost the same as that of the DSLM scheme. When U is equal to 4 or 8, the C-DSLM scheme's performance is only approximately 0.25 dB below that of the DSLM scheme. However, for the given values of U, the multiplication complexity of our proposed C-DSLM scheme is only approximately 25% or 12.5%, respectively, that of the DSLM scheme. Therefore, the C-DSLM scheme proposed in this paper is a very practical SLM framework with good application prospects.

B. Impact of the Variation of the Duration T_0

Due to the overlapping structure of FBMC signals, the duration T_0 of the PAPR of the FBMC signal has an important influence on the performance of SLM-based PAPR reduction schemes, which has been analyzed in detail in Section II-B. Fig. 9 shows the CCDF curves of the PAPR of the FBMC signal suppressed using the C-DSLM scheme for different durations T_0. When $T_0 = [0, 1T]$, that is, without considering the overlapping structure of the FBMC signal, the C-DSLM scheme has almost no effect on the PAPR regardless of the size of U, which is an expected result. The PAPR reduction performance of the C-DSLM scheme is almost the same for

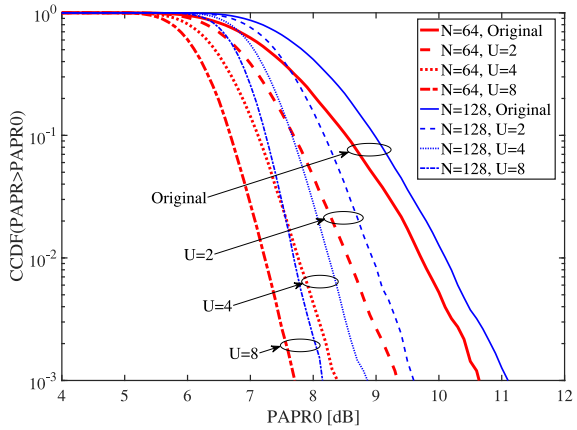

Fig. 10. CCDFs of the proposed C-DSLM scheme for different values of N, $U = \{2, 4, 8\}$, and $O = 4$.

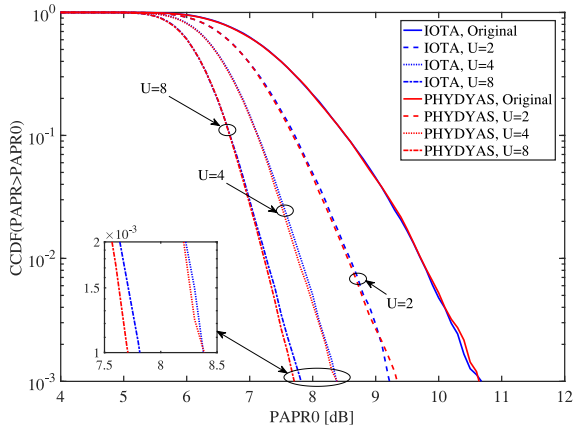

Fig. 11. CCDFs of the C-DSLM scheme for different prototype filters, i.e., PHYDYAS and IOTA; $U = \{2, 4, 8\}$, $N = 64$ and $O = 4$.

$T_0 = [1T, 3T]$ and $T_0 = [0, 4T]$, regardless of whether U is set to 2, 4 or 8. This result confirms that the energy of the current FBMC symbol superimposed with the previous symbols is mainly concentrated in the interval $[1T, 3T]$.

C. Impact of the Number of Subcarriers N

An FBMC signal is a superposition of many subcarriers with different frequencies, different phases and different amplitudes. There is an intuitive relationship here; that is, the more subcarriers there are, the greater the PAPR. The CCDFs for the PAPR of the original FBMC signal in Fig. 10 show this obvious relationship. When the CCDF = 10^{-3} and the number of subcarriers N is 64 or 128, the C-DSLM scheme produces a PAPR suppression effect of 2.93 dB or 2.96 dB, respectively, compared with the original FBMC signal ($U = 8$). From another perspective, there is only a 0.03 dB gap between the gain obtained by the C-DSLM scheme when the number of subcarriers N is 64 versus 128. This result shows that our proposed C-DSLM scheme is almost independent of N and reduces the PAPR well for FBMC signals.

D. Impact of the Prototype Filter

As mentioned in Section II-A, the prototype filter affects the time-frequency focusing characteristics of an FBMC signal.

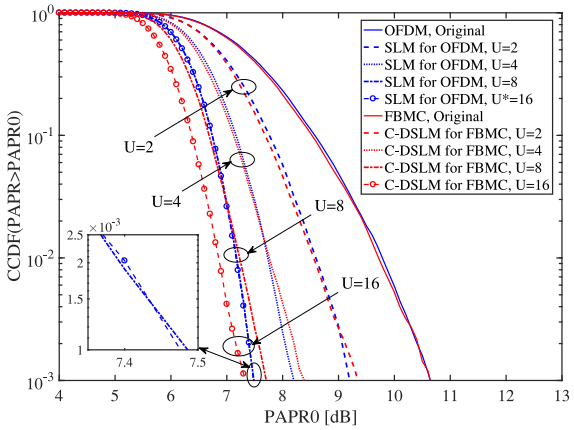

Fig. 12. PAPR reduction performance of our proposed C-DSLM scheme for an FBMC signal and the conventional SLM scheme for an OFDM signal, $N = 64$ and $O = 4$.

In view of this, here, we simulate the impact of the prototype filter on the performance of the C-DSLM scheme in terms of PAPR suppression. Fig. 11 shows the CCDFs of the PAPR of an FBMC signal suppressed by the C-DSLM scheme with PHYDYAS and IOTA filters. The results indicate that our proposed C-DSLM scheme is not sensitive to the difference between the two prototype filters and that it reduces the PAPR well regardless of which filter is employed by the FBMC system.

E. Comparison With the SLM Scheme for OFDM Systems

Finally, we compare the PAPR reduction performance of our proposed C-DSLM scheme for FBMC systems to that of the conventional SLM scheme designed for OFDM systems in Fig. 12. The C-DSLM scheme for FBMC systems performs similarly to the SLM scheme for OFDM systems in terms of PAPR reduction. When $U = 8$, there is only a gap of 0.22 dB between them, and the gap decreases to 0.18 dB when $U = 4$. In addition, we conducted an interesting experiment to verify the prediction mentioned in Section IV-A. When $U = 16$ (when 8 phase rotation vectors are obtained by inverting the sign of the other 8 phase rotation vectors), the SLM scheme does not exhibit any performance gain over the performance when $U = 8$; however, the C-DSLM scheme exhibits a PAPR suppression performance gain of 0.37 dB.

VI. Conclusion

We propose a conversion vector-based low-complexity dispersive selection mapping (DSLM) scheme to reducing the PAPR of FBMC signals in this paper. This scheme is called the C-DSLM scheme. In the C-DSLM scheme, candidate FBMC signals are generated by multiplying the original signal by the cyclic shift of the conversion vectors. The process of generating an alternate signal requires only a few complex addition operations. An evaluation of the complexity and simulation results show that compared with the DSLM scheme, the C-DSLM scheme provides similar PAPR suppression performance with much less computational complexity.

Therefore, our proposed C-DSLM scheme is a very practical SLM-based PAPR reduction scheme with good application prospects.

ACKNOWLEDGMENT

The authors would like to thank the Editor and the anonymous reviewers for their precious time and valuable comments.

REFERENCES

[1] R. Nissel, S. Schwarz, and M. Rupp, "Filter bank multicarrier modulation schemes for future mobile communication," *IEEE J. Sel. Areas Commun.*, vol. 35, no. 8, pp. 1768–1782, Aug. 2017.

[2] D. Chen, Y. Tian, D. Qu, and T. Jiang, "OQAM-OFDM for wireless communications in future Internet of Things: A survey on key technologies and challenges," *IEEE Internet Things J.*, vol. 5, no. 5, pp. 3788–3809, Oct. 2018.

[3] R. T. Kobayashi and T. Abrão, "FBMC prototype filter design via convex optimization," *IEEE Trans. Veh. Technol.*, vol. 68, no. 1, pp. 393–404, Jan. 2019.

[4] J. Choi, Y. Oh, H. Lee, and J. Seo, "Pilot-aided channel estimation utilizing intrinsic interference for FBMC/OQAM systems," *IEEE Trans. Broadcast.*, vol. 63, no. 4, pp. 644–655, Dec. 2017.

[5] J. Li, D. Chen, D. Qu, Y. Zhang, and T. Jiang, "Receiver design for Alamouti coded FBMC system in highly frequency selective channels," *IEEE Trans. Broadcast.*, vol. 65, no. 3, pp. 601–608, Sep. 2019.

[6] L. Zhang, P. Xiao, A. Zafar, A. U. Quddus, and R. Tafazolli, "FBMC system: An insight into doubly dispersive channel impact," *IEEE Trans. Veh. Technol.*, vol. 66, no. 5, pp. 3942–3956, May 2017.

[7] Y. Tian, D. Chen, K. Luo, and T. Jiang, "Prototype filter design to minimize stopband energy with constraint on channel estimation performance for OQAM/FBMC systems," *IEEE Trans. Broadcast.*, vol. 65, no. 2, pp. 260–269, Jun. 2019.

[8] A. J. Al-Dweik, "A novel non-data-aided symbol timing recovery technique for OFDM systems," *IEEE Trans. Commun.*, vol. 54, no. 1, pp. 37–40, Jan. 2006.

[9] A. Al-Dweik, S. Younis, A. Hazmi, C. Tsimenidis, and B. Sharif, "Efficient OFDM symbol timing estimator using power difference measurements," *IEEE Trans. Veh. Technol.*, vol. 61, no. 2, pp. 509–520, Feb. 2012.

[10] B. Kwon, S. Kim, D. Jeon, and S. Lee, "Iterative interference cancellation and channel estimation in evolved multimedia broadcast multicast system using filter-bank multicarrier-quadrature amplitude modulation," *IEEE Trans. Broadcast.*, vol. 62, no. 4, pp. 864–875, Dec. 2016.

[11] X. Cheng, D. Liu, C. Wang, S. Yan, and Z. Zhu, "Deep learning based channel estimation and equalization scheme for FBMC/OQAM systems," *IEEE Wireless Commun. Lett.*, vol. 8, no. 3, pp. 881–884, Jun. 2019.

[12] W. Li, D. Qu, and T. Jiang, "An efficient preamble design based on comb-type pilots for channel estimation in FBMC/OQAM systems," *IEEE Access*, vol. 6, pp. 64698–64707, 2018.

[13] A. Skrzypczak, P. Siohan, and J. Javaudin, "Analysis of the peak-to-average power ratio for OFDM/OQAM," in *Proc. IEEE Workshop Signal Process. Adv. Wireless Commun. (SPAWC)*, 2006, pp. 1–5.

[14] T. Jiang and Y. Wu, "An overview: Peak-to-average power ratio reduction techniques for OFDM signals," *IEEE Trans. Broadcast.*, vol. 54, no. 2, pp. 257–268, Jun. 2008.

[15] Y. Rahmatallah and S. Mohan, "Peak-to-average power ratio reduction in OFDM systems: A survey and taxonomy," *IEEE Commun. Surveys Tuts.*, vol. 15, no. 4, pp. 1567–1592, 4rd Quart., 2013.

[16] X. D. Li and L. J. Cimini, "Effect of clipping and filtering on the performance of OFDM," *IEEE Commun. Lett.*, vol. 2, no. 5, pp. 131–133, May 1998.

[17] X. Wang, T. T. Tjhung, and C. S. Ng, "Reduction of peak-to-average power ratio of OFDM system using a companding technique," *IEEE Trans Broadcast.*, vol. 45, no. 3, pp. 303–307, Sep. 1999.

[18] S. H. Muller and J. B. Huber, "OFDM with reduced peak-to-average power ratio by optimum combination of partial transmit sequences," *Electron. Lett.*, vol. 33, no. 5, pp. 368–369, 1997.

[19] R. W. Bauml, R. F. H. Fischer, and J. B. Huber, "Reducing the peak-to-average power ratio of multicarrier modulation by selected mapping," *Electron. Lett.*, vol. 32, no. 22, pp. 2056–2057, Oct. 1996.

[20] J. Tellado and J. M. Cioffi, "Peak power reduction for multicarrier transmission," in *Proc. IEEE GLOBECOM*, Dec. 1998, pp. 731–735.

[21] A. E. Jones, T. A. Wilkinson, and S. K. Barton, "Block coding scheme for reduction of peak to mean envelope power ratio of multicarrier transmission schemes," *Electron. Lett.*, vol. 30, no. 25, pp. 2098–2099, Dec. 1994.

[22] D. Wulich, "Reduction of peak to mean ratio of multicarrier modulation using cyclic coding," *Electron. Lett.*, vol. 32, no. 5, pp. 432–433, 1996.

[23] T. Jiang and X. Li, "Using fountain codes to control the peak-to-average power ratio of OFDM signals," *IEEE Trans. Veh. Technol.*, vol. 59, no. 8, pp. 3779–3785, Oct. 2010.

[24] Z. Kollar and P. Horvath, "PAPR reduction of FBMC by clipping and its iterative compensation," *J. Comput. Netw. Commun.*, vol. 5, Jun. 2012, Art. no. 382736.

[25] Z. You, I.-T. Lu, R. Yang, and J. L. Li, "Flexible companding design for PAPR reduction in OFDM and FBMC systems," in *Proc. Int. Conf. Comput. Netw. Commun. (ICNC)*, San Diego, CA, USA, 2013, pp. 408–412.

[26] D. Qu, S. Lu, and T. Jiang, "Multi-block joint optimization for the peak-to-average power ratio reduction of FBMC-OQAM signals," *IEEE Trans. Signal Process.*, vol. 61, no. 7, pp. 1605–1613, Apr. 2013.

[27] C. Ye, Z. Li, T. Jiang, C. Ni, and Q. Qi, "PAPR reduction of OQAM-OFDM signals using segmental PTS scheme with low complexity," *IEEE Trans. Broadcast.*, vol. 60, no. 1, pp. 141–147, Mar. 2014.

[28] A. Hanprasitkum, A. Numsomran, P. Boonsrimuang, and P. Boonsrimuang, "Improved PTS method with new weighting factor technique for FBMC-OQAM systems," in *Proc. 19th Int. Conf. Adv. Commun. Technol. (ICACT)*, 2017, pp. 143–147.

[29] Z. He, L. Zhou, Y. Chen, and X. Ling, "Low-complexity PTS scheme for PAPR reduction in FBMC-OQAM systems," *IEEE Commun. Lett.*, vol. 22, no. 11, pp. 2322–2325, Nov. 2018.

[30] A. Skrzypczak, J.-P. Javaudin, and P. Siohan, "Reduction of the peak-to-average power ratio for the OFDM/OQAM modulation," in *Proc. IEEE Veh. Technol. Conf. (VTC)*, 2006, PP. 2018–2022.

[31] Y. Zhou, T. Jiang, C. Huang, and S. Cui, "Peak-to-average power ratio reduction for OFDM/OQAM signals via alternative-signal method," *IEEE Trans. Veh. Technol.*, vol. 63, no. 1, pp. 494–499, Jan. 2014.

[32] S. S. K. C. Bulusu, H. Shaiek, D. Roviras, and R. Zayani, "PAPR reduction for FBMC-OQAM systems using dispersive SLM technique," in *Proc. 11th IEEE Int. Symp. Wireless Commun. Syst. (ISWCS)*, 2014, pp. 568–572.

[33] S. S. K. C. Bulusu, H. Shaiek, and D. Roviras, "Potency of trellis-based SLM over symbol-by-symbol approach in reducing PAPR for FBMC-OQAM signals," in *Proc. IEEE Int. Commun. Conf. (ICC)*, London, U.K., May 2015, pp. 4757–4762.

[34] M. Laabidi, R. Zayani, and R. Bouallegue, "A novel multi-block selective mapping scheme for PAPR reduction in FBMC/OQAM systems," in *Proc. World Congr. Inf. Technol. Comput. Appl. (WCITCA)*, 2015, pp. 1–5.

[35] S. S. K. C. Bulusu, H. Shaiek, and D. Roviras, "Reducing the PAPR in FBMC-OQAM systems with low-latency trellis-based SLM technique," *EURASIP J. Adv. Signal Process.*, vol. 13, no. 1, pp. 132–142, Jan. 2016.

[36] H. Wang, X. Wang, L. Xu, and W. Du, "Hybrid PAPR reduction scheme for FBMC/OQAM systems based on multi data block PTS and TR methods," *IEEE Access*, vol. 4, pp. 4761–4768, 2016.

[37] J. Zhao, S. Ni, and Y. Gong, "Peak-to-average power ratio reduction of FBMC/OQAM signal using a joint optimization scheme," *IEEE Access*, vol. 5, pp. 15810–15819, 2017.

[38] J.-H. Moon, Y. R. Nam, and J. H. Kim, "PAPR reduction in the FBMC-OQAM system via segment-based optimization," *IEEE Access*, vol. 6, pp. 4994–5002, 2018.

[39] V. Sundeepkumar and S. Anuradha, "Adaptive clipping-based active constellation extension for PAPR reduction of OFDM/OQAM signals," *Circuits Syst. Signal Process.*, vol. 36, no. 7, pp. 3034–3046, Jul. 2017.

[40] S. Ren, H. Deng, X. Qian, and Y. Liu, "Sparse PTS scheme based on TR schemes for PAPR reduction in FBMC-OQAM systems," *IET Commun.*, vol. 12, no. 14, pp. 1722–1727, 2018.

[41] L. Mounira and B. Ridha, "A joint use of both PAPR reduction and neural network predistortion approaches to compensate the HPA non-linearity impact on FBMC/OQAM signals," *Wireless Pers. Commun.*, vol. 100, no. 5, pp. 1851–1866, May 2018.

[42] K. Chen-Hu, J. C. Estrada-Jiménez, M. J. F. García, and A. G. Armada, "Continuous and burst pilot sequences for channel estimation in FBMC-OQAM," *IEEE Trans. Veh. Technol.*, vol. 67, no. 10, pp. 9711–9720, Oct. 2018.

[43] M. Bellanger, "Specification and design of prototype filter for filter bank based multicarrier transmission," in *Proc. IEEE Int. Conf. Acoust. Speech Signal Process. (ICASSP)*, May 2001, pp. 2417–2420.

[44] E. Al-Dalakta, A. Al-Dweik, A. Hazmi, C. Tsimenidis, and B. Sharif, "Efficient BER reduction technique for nonlinear OFDM transmission using distortion prediction," *IEEE Trans. Veh. Technol.*, vol. 61, no. 5, pp. 2330–2336, Jun. 2012.
[45] E. Al-Dalakta, A. Al-Dweik, A. Hazmi, C. Tsimenidis, and B. Sharif, "PAPR reduction scheme using maximum cross correlation," *IEEE Commun. Lett.*, vol. 16, no. 12, pp. 2032–2035, Dec. 2012.
[46] C.-L. Wang, M. Y. Hsu, and Y. Ouyang, "A low-complexity peak-to-average power ratio reduction technique for OFDM systems," in *Proc. IEEE GLOBECOM*, San Francisco, CA, USA, Dec. 2003, pp. 2375–2379.
[47] C.-L. Wang and Y. Ouyang, "Low-complexity selected mapping schemes for peak-to-average power ratio reduction in OFDM systems," *IEEE Trans. Signal Process.*, vol. 53, no. 12, pp. 4652–4660, Dec. 2005.
[48] C.-L. Wang and S.-J. Ku, "Novel conversion matrices for simplifying the IFFT computation of an SLM-based PAPR reduction scheme for OFDM systems," *IEEE Trans. Commun.*, vol. 57, no. 7, pp. 1903–1907, Jul. 2009.
[49] C.-P. Li, S.-H. Wang, and C.-L. Wang, "Novel low-complexity SLM schemes for PAPR reduction in OFDM systems," *IEEE Trans. Signal Process.*, vol. 58, no. 5, pp. 2916–2921, May 2010.
[50] M. S. Ahmed, S. Boussakta, A. J. Al-Dweik, B. Sharif, and C. C. Tsimenidis, "Efficient design of selective mapping and partial transmit sequence using T-OFDM," *IEEE Trans. Veh. Technol.*, early access, doi: 10.1109/TVT.2019.2928361.

Xing Cheng (Member, IEEE) was born in Wuhan, China, in 1989. He received the Ph.D. degree from the China University of Petroleum, Beijing, in 2019. He is currently a Lecturer with the School of Information and Communication Engineering, Beijing Information Science and Technology University, Beijing. His research interests include detection, control and optimization of complex systems, OFDM system, FBMC system, the application of deep learning technology in the communication physical layer, and logging cable-based high-speed teletransmission system.

Dejun Liu (Member, IEEE) was born in Hebei, China, in 1965. He received the Ph.D. degree in instrumentation science and technology from the Harbin Institute of Technology, Harbin, China, in 2001. He joined the Electrical Engineering Department, Daqing Petroleum Institute, Heilongjiang, China, where he was an Associate Professor of instrumentation science and technology until 2002. He is currently a Professor with the College of Information Science and Engineering, China University of Petroleum, Beijing, China. He has published about 140 scientific papers. His research interests include intelligent instrumentation and automatic measuring system, measurement theory, logging cable-based high-speed teletransmission system, and virtual prototype design for electromechanical measurement system.

Wenzhe Shi was born in Beijing, China, in 1996. She received the B.S. degree in electrical engineering from Beijing Information Science and Technology University, Beijing, in 2017. She is currently pursuing the M.S. degree with the Department of College of Information Science and Engineering, China University of Petroleum, Beijing. Her research interests include communication theory, modulation and demodulation, and the application of deep learning technology in the communication physical layer.

Yang Zhao was born in Hebei, China, in 1995. He received the B.S. degree in electrical engineering from Northeast Petroleum University, Daqing, China, in 2017. He is currently pursuing the M.S. degree with the Department of College of Information Science and Engineering, China University of Petroleum, Beijing, China. His research interests include communication theory, OFDM system, channel estimation and equalization, and the application of deep learning technology in the communication physical layer.

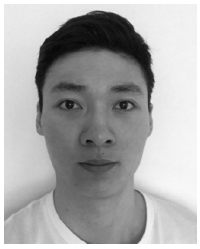

Yang Li was born in Hebei, China, in 1994. He received the B.S. degree in electrical engineering from Northeast Petroleum University, Daqing, China, in 2017. He is currently pursuing the M.S. degree with the Department of College of Information Science and Engineering, China University of Petroleum, Beijing. His research interests include the application of deep learning technology in the communication physical layer and identification of fractures in oil and gas reservoirs.

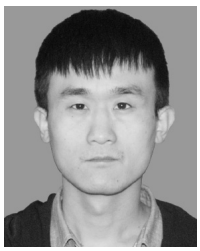

Dejin Kong received the B.S. and Ph.D. degrees from the Huazhong University of Science and Technology, Wuhan, China, in 2011 and 2016, respectively. He is currently working with Wuhan Textile University. His current research interests include the areas of wireless communications, especially for FBMC, OFDM, and MIMO.